THE JOURNAL OF PHYSICAL CHEMISTRY Letters

Letter

pubs.acs.org/JPCL

Photoinduced Giant Dielectric Constant in Lead Halide Perovskite Solar Cells

Emilio J. Juárez-Pérez,[†] Rafael S. Sánchez,[†] Laura Badia,[†] Germá Garcia-Belmonte,[†] Yong Soo Kang,[‡] Ivan Mora-Sero,*[,†] and Juan Bisquert*[,†,§]

[†]Photovoltaics and Optoelectronic Devices Group, Departament de Fisica, Universitat Jaume I, 12071 Castello, Spain

[‡]Center for Next Generation Dye-sensitized Solar Cells, Department of Energy Engineering, Hanyang University, Seoul 133-791, South Korea

[§]Department of Chemistry, Faculty of Science, King Abdulaziz University, Jeddah 21589, Saudi Arabia

Supporting Information

ABSTRACT: Organic−inorganic lead trihalide perovskites have emerged as an outstanding photovoltaic material that demonstrated a high 17.9% conversion efficiency of sunlight to electricity in a short time. We have found a giant dielectric constant (GDC) phenomenon in these materials consisting on a low frequency dielectric constant in the dark of the order of ε_0 = 1000. We also found an unprecedented behavior in which ε_0 further increases under illumination or by charge injection at applied bias. We observe that ε_0 increases nearly linearly with the illumination intensity up to an additional factor 1000 under 1 sun. Measurement of a variety of samples of different morphologies, compositions, and different types of contacts shows that the GDC is an intrinsic property of $MAPbX_3$. We hypothesize that the large dielectric response is induced by structural fluctuations. Photoinduced carriers modify the local unit cell equilibrium and change the polarizability, assisted by the freedom of rotation of $CH_3NH_3^+$. The study opens a way for the understanding of a key aspect of the photovoltaic operation of high efficiency perovskite solar cells.

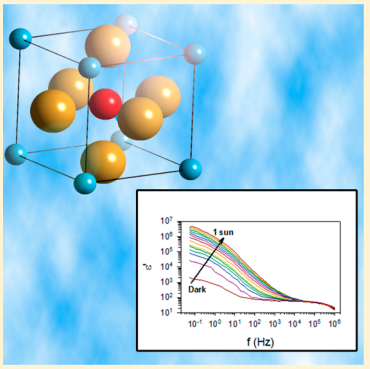

SECTION: Energy Conversion and Storage; Energy and Charge Transport

Perovskite solar cells have emerged as a major topic of research in photovoltaics because of the promising properties of the solution processed, low cost, and high efficiency solar cells for large-scale solar energy production.[1,2] Perovskite is the denomination for any material with the general chemical formula ABX_3 that adopts the crystalline structure of calcium titanate, $CaTiO_3$. Compositional combinations provide hundreds of materials with perovskite structure, and many display a fascinating variety of electric, piezoelectric, and electro-optical properties, such as high polar behavior and structural and ferroelectric phase transitions.[3,4] These last properties rely on a complex interplay between the substitutional chemistry and the lattice displacements.[5,6]

Since the 1990s, organic−inorganic hybrid halide perovskites have been investigated for their promising semiconductor properties.[7] Recently, photovoltaic behavior was discovered using the methylammonium lead trihalide perovskite ($MAPbX_3$, MA = $CH_3NH_3^+$; X_3 = Br_3, I_3, $I_{3-x}Cl_x$) as light absorber[8,9] and further developments in the last two years reached nearly 18% conversion efficiency of sunlight to electricity that already overcomes the performance of some established thin film photovoltaic technologies.[10−12] These results have boosted the research on these materials to further improve their photovoltaic efficiencies. Consequently, there is a growing interest to understand the detailed physical properties of $MAPbX_3$ perovskites in order to develop better photovoltaic structures as well as new applications of these semiconductors. We have conducted a number of studies of their electrical and electro-optical properties that have provided basic insights to the photovoltaic mechanisms.[13,14] Here, we report an outstanding and unique physical behavior in the photovoltaic classes of materials, a carrier-induced giant dielectric constant (GDC). The large dielectric relaxation is a central element to understand the physical processes in the perovskite photovoltaic devices[15] and opens up these materials for unexpected new applications.

The structure of the perovskite plays a significant role in the observed phenomena.[16−18] In the high temperature cubic phase, it has a B cation in 6-fold coordination with an octahedron of X anions (a corner sharing $[BX_6]$ octahedra) and the A cation occupying the 12-fold cuboctahedral coordination site. Under application of stress or electrical field, two main distortions can be distinguished: a polar displacement of both A and X atoms (off-centering), or a nonpolar rotation of $[BX_6]$ octahedra. In many cubic materials, off-centering leads to a ferroelectric phase transition, but in a majority of perovskites,

Received: June 3, 2014
Accepted: June 23, 2014

   dx.doi.org/10.1021/jz5011169 | J. Phys. Chem. Lett. XXXX, XXX, XXX−XXX

the $[BX_6]$ octahedra are tilted and they are not ferroelectric. In contrast with oxide based perovskites, the halide perovskites as $MAPbI_3$ show the cubic symmetry phase transition at relatively low temperature, 56 °C, and the tetragonal lattice, Figure 1b, is

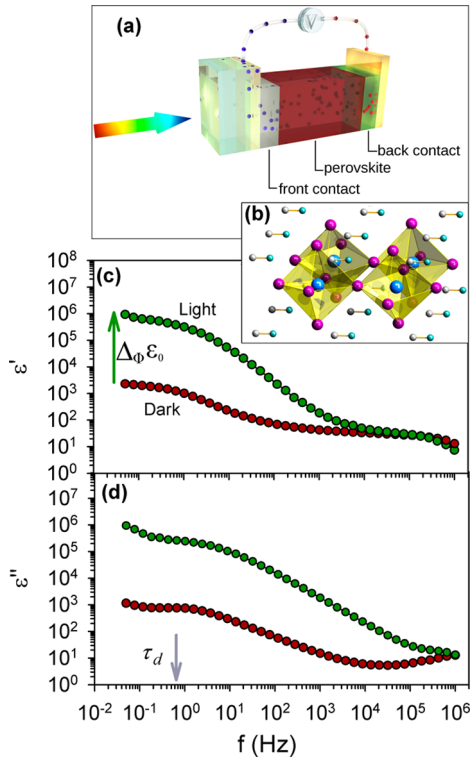

Figure 1. (a) Scheme of the experimental devices; the arrow indicates light incident side. (b) Tetragonal perovskite, phase at room temperature; the blue sphere is the B cation (Pb^{2+}), the crimson color spheres represent the X anion, and white and cyan spheres represent C and N atoms from MA. (c) Real and (d) imaginary part of dielectric permittivity as a function of frequency under dark and 1 sun illumination conditions, measured at room temperature and 0 V applied bias, for thin film of SnO_2:F (FTO)/compact TiO_2/$MAPbI_{3-x}Cl_x$ perovskite in Al_2O_3 scaffold/spiro-OMeTAD/Au.

maintained until −112 °C when it undergoes phase transition to orthorrombic phase, Supporting Information Figure SI1. Very recently, Frost et al. have discussed theoretically the presence of ferroelectric domains in $MAPbI_3$.[19]

GDC is observed in materials in which the low frequency limit of the real part of the dielectric constant becomes large, $\varepsilon_0 > 1000$. Provided that ε_0 shows small temperature dependence, these materials are applied to high dielectric constant capacitors for energy or memory storage devices. GDC was suggested in polaronic conductors as a possible cause for high T_c superconductivity,[20] and it has also been reported for inorganic and hybrid metal oxide perovskites[21,22] and in molecular crystals.[23] The origin of GDC in several classes of materials is a subject of debate, as it can be ascribed to different causes, namely, an intrinsically high polarizability due to either ionic displacements or to dipolar or hopping contributions of polarons,[20,24] or alternatively, morphology features as interfacial polarization at the insulating boundaries between semiconducting grain or polarization at the metal/dielectric interface.[25,26] In either case, in the previous literature reports the GDC is caused by inherent electronic carriers in the material, whereas a photoinduced effect has been only rarely observed.[27] Below, we report the observation of GDC in $MAPbX_3$ perovskites that can be achieved by injection of carriers induced either by photogeneration or applied voltage, in a diode structure.

At present, there are two main kinds of perovskite photovoltaic films where $MAPbX_3$ is deposited inside of a metal oxide nanostructured scaffold that may be semiconducting (TiO_2)[10,28] or an insulator (Al_2O_3)[29] and alternatively as planar film without scaffold.[11,30] We prepared a variety of films on these configurations, see Figure 1a, using different contacts combinations: (i) diode (solar cell) structure, with asymmetric electron and hole selective contacts, (ii) symmetric contacts that allow injection of only one kind of carrier, either electrons or holes, and (iii) films with blocking insulator layers that prevent carrier injection. The dielectric constant $\varepsilon(\omega) = \varepsilon' - i\varepsilon''$ was measured as a function of frequency under different conditions of bias voltage, illumination, and temperature. The experimental details of materials, device preparation and their characterization measurements are described in Supporting Information.

The characteristic behavior of the frequency dependent real part of the dielectric constant is shown in Figure 1c. In the dark, the permittivity of the perovskite film decreases from a low frequency value of about $\varepsilon_0 \approx 1000$, showing already GDC, to the high frequency value ε_∞ in the order of tens. The decrease of ε' shows a number of features. A relaxation peak is observed in the dielectric loss ε'' at the frequency $f_d = 0.5$ Hz, and it can be ideally described by the generic Debye expression

$$\varepsilon(\omega) = \varepsilon_\infty + \frac{\varepsilon_0 - \varepsilon_\infty}{1 + i\omega\tau_d} \quad (1)$$

where $\tau_d = (2\pi f_d)^{-1}$ is a temperature-dependent constant, the relaxation time. At the high frequency side of the ε'' peak, the real part of the permittivity (associated with the system's capacitance) does not abruptly decay as would be expected from eq 1. This feature is related, on one hand, to the presence of a capacitance not related to dielectric polarization, to the chemical capacitance[31] that has been emphasized in a previous report,[13] and in addition, to a distribution of relaxation times which gives rise to well-known dielectric functions can also contribute to the smoothness in the ε' step. Due to the effect of the dc conductance, the dielectric loss ε'' increases at the low frequency side of the relaxation peak at τ_d. Identical features have been observed either with TiO_2 scaffold or with no scaffold, Supporting Information Figure SI2. Also, with different contacts, symmetric, asymmetric or blocking, see Supporting Information Figure SI3. Furthermore, GDC is not exclusive of the $MAPbI_{3-x}Cl_x$ perovskite and it has been also observed for $CH_3NH_3PbI_3$, see Supporting Information Figure SI4.

Illumination of the perovskite samples produces a significant increase of charge carrier density in the perovskite layer due to the high extinction coefficient of organic−inorganic lead halide perovskite.[17] Figure 1c shows that upon application of 1 sun illumination intensity to the sample, ε_∞ is not modified but there is a prodigious shift of the permittivity from intermediate to low frequencies that produces a change of the dielectric constant until a plateau is attained at values as high as $\varepsilon_0 \approx 10^6$−$10^7$ implying a photoinduced variation of factor ≈1000. Dependence of the permittivity vs incident light intensity, Φ_0, is further analyzed in Figure 2, that shows a relationship $\varepsilon_0 = k(\Phi_0)^\gamma$ with $\gamma = 1.1$.

In order to discriminate between bulk and interfacial effect, different contact configurations have been explored, including the diode structure, the blocking of one of the contacts, and

dx.doi.org/10.1021/jz5011169 | J. Phys. Chem. Lett. XXXX, XXX, XXX−XXX

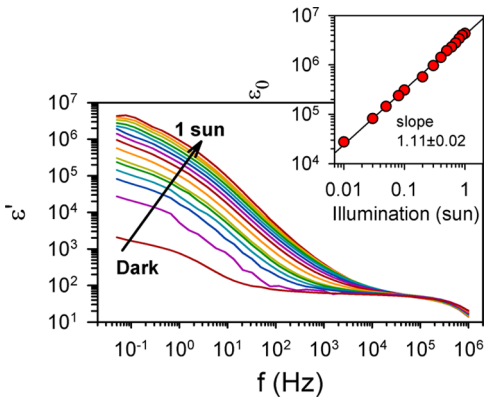

Figure 2. Plot of the real permittivity as a function of frequency for different incident light intensity (Φ_0) from dark to 1 sun, for $MAPbI_{3-x}Cl_x$ perovskite (compact TiO_2/ $MAPbI_{3-x}Cl_x$ perovskite in Al_2O_3 scaffold/spiro-OMeTAD). Measurements have been carried out at room temperature and 0 V applied bias. Inset, linear regression of dielectric constant vs illumination intensity at f = 50 mHz, observing a close to linear dependence between ε_0 and intensity illumination.

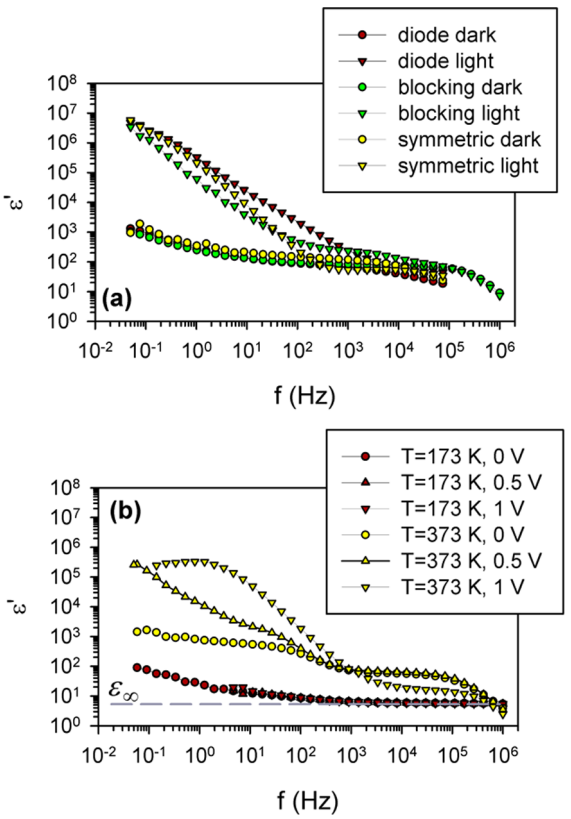

Figure 3. Plots of the real part of dielectric permittivity as a function of frequency. (a) Under dark and 1 sun illumination for thin film of $CH_3NH_3PbI_{3-x}Cl_x$ perovskite without scaffold, with spiro-OMeTAD as back contact, using different front contacts: TiO_2 (diode device); thin CaO ~20 nm isolating layer (blocking device) and spiro-OMeTAD (symmetric device). Measurements have been carried out at room temperature and 0 V applied bias. (b) At different temperatures and three different applied bias conditions for thin film of perovskite without scaffold and using asymmetric contacts: compact TiO_2/$CH_3NH_3PbI_{3-x}Cl_x$/spiro-OMeTAD. Measurements have been carried out under dark conditions.

f3

symmetric contacts, see Figure 3a and Supporting Information Figure SI3. The effect of front contact (illumination side) can be appreciated only at high and intermediate frequencies.[32] However, at low frequency when GDC is observed, ε' values are independent of front contact. A similar trend is observed for ε' when the back contact is modified, see Supporting Information Figure SI3. The increase of GDC observed cannot be attributed to an effect related with the photocurrent as it is also obtained when blocking contacts (20 nm of CaO) are inserted in the front or in the back contact. In this sense, the independence of the phenomena with the kind of contact suggests an intrinsic effect related with bulk perovskite. The application of bias voltage at room temperature, from 0 to 1 V, with this last value being similar to the photovoltage in the solar cell at 1 sun, increases markedly, the ε' and finally provokes a similar GDC effect to that of photogeneration, see Supporting Information Figure SI5. These results point to a direct relation between the charge carrier density and the increase of the giant permittivity, which indistinctly occurs due either to photogeneration or to carrier injection by applied bias.

Voltage and temperature dependence of the GDC effect are analyzed in Figure 3b and Supporting Information Figures SI5 and SI6. At 0 V and low temperature, a relative permittivity of $\varepsilon_\infty \approx 7$ is observed at high and intermediate frequencies. This is a realistic value for the geometric dielectric permittivity of the sample, considering that a value of 7.1 has been recently calculated for the $CH_3NH_3PbI_3$ perovskite.[33] At high T, a richer permittivity pattern is obtained, Figure 3b. There is a first step at high frequency bringing ε' to values ~100 in a thermally activated process. This increase of ε' should be related with a capacitance at the contacts.[32] At temperature of 273 K and higher, see Supporting Information Figure SI6, a second step appears that increases real permittivity to 10^3−10^4. Finally, a third step appears at low frequency promoting real permittivity to high GDC of 10^5−10^6. Results in Figure 3 confirm that the giant dielectric permittivity is related with the increase in carrier density due to illumination, charge injection, or temperature. Although the dielectric permittivity has been previously studied for these perovskite materials, there are no reports of studies under illumination or at frequencies as low as the analyzed in this paper, and consequently GDC has not been previously reported. Nevertheless, previous results of ε' as high as 200 have been reported for X = (Cl, Br) perovskite single crystals at 50 Hz.[34] These values are in the range of the results shown here.

In summary, the large number of samples investigated, with a wide variation of internal morphologies, compositions, and contacts, including samples with insulating contacts, show the GDC effect in all cases. Therefore, it is reasonable to assume that the large dielectric constant is an intrinsic effect related to increased population of electronic carriers and not an interfacial one.

Already in the dark (without added carriers), the perovskite shows a very large static dielectric constant. This feature reflects the response of small dipolar domains to the external electrical field. The large native dielectric constant could be induced by structural fluctuations of the perovskite cell, aided by the large freedom of rotation of the polar $CH_3NH_3^+$ cation.[32,33] The dipole−dipole interaction is weak so that the correlation length ξ_c of the dipolar domains may comprise only a few unit cells.[15] These domains tend to align to the external field. According to our observations, when carriers are injected, an enhanced polarizability is induced by electronic carriers located in the conduction band and holes in the valence band, corresponding

dx.doi.org/10.1021/jz5011169 | J. Phys. Chem. Lett. XXXX, XXX, XXX−XXX

in the first case to the hybridizations of the 6p orbitals of B (lead) and to hybridizations of the 6s orbitals of B and 5p orbitals of X (halide) for the valence band.[34] However, in a highly polar crystal, the electronic carriers become strongly localized by electron−phonon coupling. The self-stabilized electronic charge in a deformable polar medium is termed a polaron, and its slow motion, which drags the lattice distortion, is denoted polaron hopping. The presence of excess localized charge, with a relative positional freedom to move under external or thermal force, modifies the ionic bonding balance of the unit cell and causes local distortion. Previous experimental results[35−38] reveal a high mobility of carriers but those measurements are obtained at 10^9 Hz which is 9 orders of magnitude faster than the dynamic polarization observed here. Terahertz conductivity only probes the electronic carrier dynamics in a very short scale vibrational motion. The carrier-induced enhanced polarization is on a very slow scale of 1 Hz, as it involves the macroscopic rearrangement of dipolar domains, and it will influence the long-range carrier transport. Indeed, it can be observed in Supporting Information Figure SI2 that the low frequency conductivity decreases by 2 orders of magnitude with respect to the intermediate frequency (1 kHz) conductivity. We remark that long-range transport may be either band-like or, in the case of polaron hopping, it will involve a small activation energy. It is also likely that different mechanisms may coexist in the inhomogeneous environment caused by the dipolar domains and grain boundaries structure. These facts could have profound implications for the electronic and photovoltaic operation of the material that will require a detailed investigation. On the other hand, it opens the possibility of development of new optoelectronic devices as photonic control of memory devices or capacitance based photodetectors.

■ ASSOCIATED CONTENT

Supporting Information

Crystalline structure, methods, dielectric relaxation data. This material is available free of charge via the Internet http://pubs.acs.org.

■ AUTHOR INFORMATION

Corresponding Authors

*I. Mora-Sero. E-mail: sero@uji.es.

*J. Bisquert. E-mail: bisquert@uji.es.

Notes

The authors declare no competing financial interest.

■ ACKNOWLEDGMENTS

This work was supported by MINECO of Spain under project MAT2013-47192-C3-1-R), Universitat Jaume I project 12I361.01/1, and National Research Foundation of Korea (NRF) grant funded by the Korea government (MSIP) (no. 2008-0061903). We thank SCIC from Universitat Jaume I for the help with SEM measurements.

■ REFERENCES

(1) Park, N.-G. Organometal Perovskite Light Absorbers Toward a 20% Efficiency Low-Cost Solid-State Mesoscopic Solar Cell. *J. Phys. Chem. Lett.* **2013**, *4*, 2423−2429.

(2) Snaith, H. J. Perovskites: The Emergence of a New Era for Low-Cost, High-Efficiency Solar Cells. *J. Phys. Chem. Lett.* **2013**, *4*, 3623−3630.

(3) Bokov, A. A. Recent Progress in Relaxor Ferroelectrics with Perovskite Structure. *J. Mater. Sci.* **2006**, *41*, 31−52.

(4) Zhong, W.; Vanderbilt, D. Competing Structural Instabilities in Cubic Perovskites. *Phys. Rev. Lett.* **1995**, *74*, 2587−2590.

(5) Ghita, M.; Fornari, M.; Singh, D. J.; Halilov, S. V. Interplay Between A-site and B-site Driven Instabilities in Perovskites. *Phys. Rev. B: Condens. Matter Mater. Phys.* **2005**, *72*, 054114.

(6) Ohtomo, A.; Muller, D. A.; Grazul, J. L.; Hwang, H. Y. Artificial Charge-Modulationin Atomic-Scale Perovskite Titanate Superlattices. *Nature* **2002**, *419*, 378−380.

(7) Mitzi, D. B. Synthesis, Structure, and Properties of Organic-Inorganic Perovskites and Related Materials. In *Progress in Inorganic Chemistry*; John Wiley & Sons, Inc.: Hoboken, NJ, 2007; pp 1−121.

(8) Kojima, A.; Teshima, K.; Shirai, Y.; Miyasaka, T. Organometal Halide Perovskites as Visible-Light Sensitizers for Photovoltaic Cells. *J. Am. Chem. Soc.* **2009**, *131*, 6050−6051.

(9) Im, J.-H.; Lee, C.-R.; Lee, J.-W.; Park, S.-W.; Park, N.-G. 6.5% Efficient Perovskite Quantum-Dot-Sensitized Solar Cell. *Nanoscale* **2011**, *3*, 4088−4093.

(10) Burschka, J.; Pellet, N.; Moon, S.-J.; Humphry-Baker, R.; Gao, P.; Nazeeruddin, M. K.; Gratzel, M. Sequential Deposition as a Route to High-Performance Perovskite-Sensitized Solar Cells. *Nature* **2013**, *499*, 316−319.

(11) Liu, M.; Johnston, M. B.; Snaith, H. J. Efficient Planar Heterojunction Perovskite Solar Cells by Vapour Deposition. *Nature* **2013**, *501*, 395−398.

(12) Wang, J. T.-W.; Ball, J. M.; Barea, E. M.; Webber, J.-A.; Hunang, J.; Mora-Sero, I.; Bisquert, J.; Snaith, H. J.; Nicholas, R. J. Low-temperature processed electron collection layers of Graphene/TiO_2 nanocomposites in thin film perovskite solar cells. *Nano Lett.* **2014**, *14*, 724−730.

(13) Kim, H.-S.; Mora-Sero, I.; Gonzalez-Pedro, V.; Fabregat-Santiago, F.; Juarez-Perez, E. J.; Park, N.-G.; Bisquert, J. Mechanism of Carrier Accumulation in Perovskite Thin-Absorber Solar Cells. *Nat. Commun.* **2013**, *4*, 2242.

(14) Gonzalez-Pedro, V.; Juarez-Perez, E. J.; Arsyad, W.-S.; Barea, E. M.; Fabregat-Santiago, F.; Mora-Sero, I.; Bisquert, J. General Working Principles of $CH_3NH_3PbX_3$ Perovskite Solar Cells. *Nano Lett.* **2014**, *14*, 888−893.

(15) Sánchez, R. S.; Gonzalez-Pedro, V.; Lee, J.-W.; Park, N.-G.; Kang, Y. S.; Mora-Sero, I.; Bisquert, J. Slow Dynamic Processes in Lead Halide Perovskite Solar Cells. Characteristic Times and Hysteresis. *J. Phys. Chem. Lett.* **2014**, DOI: 10.1021/jz5011187.

(16) Woodward, P. Octahedral Tilting in Perovskites. II. Structure Stabilizing Forces. *Acta Crystallogr., Sect. B: Struct. Sci.* **1997**, *53*, 44−66.

(17) Stoumpos, C. C.; Malliakas, C. D.; Kanatzidis, M. G. Semiconducting Tin and Lead Iodide Perovskites with Organic Cations: Phase Transitions, High Mobilities, and Near-Infrared Photoluminescent Properties. *Inorg. Chem.* **2013**, *52*, 9019−9038.

(18) Kim, H.-S.; Im, S. H.; Park, N.-G. Organolead Halide Perovskite: New Horizons in Solar Cell Research. *J. Phys. Chem. C* **2014**, *118*, 5615−5625.

(19) Frost, J. M.; Butler, K. T.; Brivio, F.; Hendon, C. H.; van Schilfgaarde, M.; Walsh, A. Atomistic Origins of High-Performance in Hybrid Halide Perovskite Solar Cells. *Nano Lett.* **2014**, *14*, 2584−2590.

(20) Samara, G. A.; Hammetter, W. F.; Venturini, E. L. Temperature and Frequency Dependences of the Dielectric Properties of $YBa_2Cu_3O_{6+x}$ (x = 0). *Phys. Rev. B: Condens. Matter Mater. Phys.* **1990**, *41*, 8974−8980.

(21) Ramirez, A. P.; Subramanian, M. A.; Gardel, M.; Blumberg, G.; Li, D.; Vogt, T.; Shapiro, S. M. Giant Dielectric Constant Response in a Copper-Titanate. *Solid State Commun.* **2000**, *115*, 217−220.

(22) Homes, C. C.; Vogt, T.; Shapiro, S. M.; Wakimoto, S.; Ramirez, A. P. Optical Response of High-Dielectric-Constant Perovskite-Related Oxide. *Science* **2001**, *293*, 673−676.

(23) Horiuchi, S.; Kumai, R.; Tokura, Y. Room-Temperature Ferroelectricity and Gigantic Dielectric Susceptibility on a Supra-

molecular Architecture of Phenazine and Deuterated Chloranilic Acid. *J. Am. Chem. Soc.* **2005**, *127*, 5010−5011.
(24) Ligatchev, V. Polaronic Phase Transitions and Complex Permittivity of Solid Polar Insulators with Gigantic Dielectric Response. *Phys. Status Solidi B* **2013**, *251*, 569−592.
(25) Lunkenheimer, P.; Bobnar, V.; Pronin, A. V.; Ritus, A. I.; Volkov, A. A.; Loidl, A. Origin of Apparent Colossal Dielectric Constants. *Phys.Rev. B* **2002**, *66*, 052105.
(26) Zhang, L.; Tang, Z.-J. Polaron Relaxation and Variable-Range-Hopping Conductivity in the Giant-Dielectric-Constant Material $CaCu_3Ti_4O_{12}$. *Phys. Rev. B: Condens. Matter Mater. Phys.* **2004**, *70*, 174306.
(27) Hasegawa, T.; Mouri, S.-I.; Yamada, Y.; Tanaka, K. Giant Photo-Induced Dielectricity in SrTiO3. *J. Phys. Soc. Jpn.* **2003**, *72*, 41−44.
(28) Kim, H.-S.; Lee, C.-R.; Im, J.-H.; Lee, K.-B.; Moehl, T.; Marchioro, A.; Moon, S.-J.; Humphry-Baker, R.; Yum, J.-H.; Moser.; et al. Lead Iodide Perovskite Sensitized All-Solid-State Submicron Thin Film Mesoscopic Solar Cell with Efficiency Exceeding 9%. *Sci. Rep.* **2012**, *2*, 591.
(29) Lee, M. M.; Teuscher, J.; Miyasaka, T.; Murakami, T. N.; Snaith, H. J. Efficient Hybrid Solar Cells Based on Meso-Superstructured Organometal Halide Perovskites. *Science* **2012**, *338*, 643−647.
(30) Liu, D.; Kelly, T. L. Perovskite Solar Cells with a Planar Heterojunction Structure Prepared Using Room-Temperature Solution Processing Techniques. *Nat. Photonics* **2014**, *8*, 133−138.
(31) Bisquert, J. Chemical Capacitance of Nanostructured Semiconductors: Its Origin and Significance for Heterogeneous Solar Cells. *Phys. Chem. Chem. Phys.* **2003**, *5*, 5360−5364.
(32) Juarez-Perez, E. J.; Wuβler, M.; Fabregat-Santiago, F.; Lakus-Wollny, K.; Mankel, E.; Mayer, T.; Jaegermann, W.; Mora-Sero, I. The Role of the Selective Contacts in the Performance of Lead Halide Perovskite Solar Cells. *J. Phys. Chem. Lett.* **2014**, *5*, 680−685.
(33) Umari, P.; Mosconi, E.; De Angelis, F. Relativistic GW calculations on $CH_3NH_3PbI_3$ and $CH_3NH_3SnI_3$ Perovskites for Solar Cell Applications. *Sci. Rep.* **2014**, *4*, 4467.
(34) Maeda, M.; Hattori, M.; Hotta, A.; Suzuki, I. Dielectric Studies of $CH_3NH_3PbX_3$ (X = Cl and Br) Single Crystals. *J. Phys. Soc. Jpn.* **1997**, *66*, 1508−1511.
(35) Wasylishen, R. E.; Knop, O.; Macdonald, J. B. Cation Rotation in Methylammonium Lead Halides. *Solid State Commun.* **1985**, *56*, 581−582.
(36) Mashiyama, H.; Kawamura, Y.; Kubota, Y. The Anti-Polar Structure of $CH_3NH_3PbBr_3$. *J. Korean Phys. Soc.* **2007**, *51*, 850−853.
(37) Even, J.; Pedesseau, L.; Jancu, J.-M.; Katan, C. Importance of Spin−Orbit Coupling in Hybrid Organic/Inorganic Perovskites for Photovoltaic Applications. *J. Phys. Chem. Lett.* **2013**, *4*, 2999−3005.
(38) Wehrenfennig, C.; Eperon, G. E.; Johnston, M. B.; Snaith, H. J.; Herz, L. M. High Charge Carrier Mobilities and Lifetimes in Organolead Trihalide Perovskites. *Adv. Mater.* **2014**, *26*, 1584−1589.